

Interplay between the $b \rightarrow sll$ anomalies and dark matter physics

Junichiro Kawamura¹, Shohei Okawa² and Yuji Omura³

¹*Department of Physics, University of Tokyo, Tokyo 113-0033, Japan*

²*Department of Physics, Nagoya University, Nagoya 464-8602, Japan*

³*Kobayashi-Maskawa Institute for the Origin of Particles and the Universe, Nagoya University, Nagoya 464-8602, Japan*

Abstract

Recently, the LHCb collaboration has reported the excesses in the $b \rightarrow sll$ processes. One of the promising candidates for new physics to explain the anomalies is the extended Standard Model (SM) with vector-like quarks and leptons. In that model, Yukawa couplings between the extra fermions and SM fermions are introduced, adding extra scalars. Then, the box diagrams involving the extra fields achieve the $b \rightarrow sll$ anomalies. It has been known that the excesses require the large Yukawa couplings of leptons, so that this kind of model can be tested by studying correlations with other observables. In this paper, we consider the extra scalar to be a dark matter (DM) candidate, and investigate DM physics as well as the flavor physics and the LHC physics. The DM relic density and the direct-detection cross section are also dominantly given by the Yukawa couplings, so that we find some explicit correlations between DM physics and the flavor physics. In particular, we find the predictions of the $b \rightarrow sll$ anomalies against the direct detection of DM.

1 Introduction

Recently, the LHCb collaboration has reported that there are deviations from the Standard Model (SM) predictions in the $b \rightarrow sll$ processes. In the experiment, the branching fractions of $B \rightarrow K^{(*)} ll$ ($l = e, \mu$) are measured, and lepton universalities and angular distributions are studied in each process. One excess is reported in the ratio between $\text{BR}(B^+ \rightarrow K^+ \mu\mu)$ and $\text{BR}(B^+ \rightarrow K^+ ee)$ in the region with $1 \text{ GeV}^2 \leq q^2 \leq 6 \text{ GeV}^2$, where q^2 is the invariant mass of two leptons in the final state [1]. The experimental result suggests the smaller value of $\text{BR}(B^+ \rightarrow K^+ \mu\mu)$ than the SM prediction, and the deviation is about 2.6σ [1]. Recently, a similar deviation is discovered in $B \rightarrow K^* \mu\mu$ [2]. The B decay to μ pair in this process is again smaller than the SM prediction. Similar indications are also reported in $B \rightarrow \phi \mu\mu$ [3] and $\Lambda_b \rightarrow \Lambda \mu\mu$ [4] in the same q^2 region. Moreover, the disagreement between the experimental results and the SM prediction of the angular distribution in $B \rightarrow K^* \mu\mu$ is also one of the longstanding issues [5, 6]. The CMS collaboration has shown the result that may be consistent with the SM prediction, but the deviation is still large in the LHCb experiment and the others. Thus, there might be some issues in the $b \rightarrow s$ transition associated with μ .

The SM predicts that namely C_7 , C_9 and C_{10} operators contribute to the $b \rightarrow sll$ processes. C_7 can not give sizable contributions to the processes, because it corresponds to the electric dipole operator that is strictly constrained by $B \rightarrow X_s \gamma$. In the region with $1 \text{ GeV}^2 \leq q^2 \leq 6 \text{ GeV}^2$, the C_9 and C_{10} operators dominantly contribute to the branching ratios. The Wilson coefficients, C_9^l and C_{10}^l , are defined as follows:

$$\mathcal{H}_{\text{eff}} = -\frac{4G_F}{\sqrt{2}} V_{tb} V_{ts}^* \frac{e^2}{16\pi^2} \{C_9^l (\bar{s}_L \gamma_\mu b_L) (\bar{l} \gamma^\mu l) + C_{10}^l (\bar{s}_L \gamma_\mu b_L) (\bar{l} \gamma^\mu \gamma_5 l) + h.c.\}. \quad (1)$$

In the SM, C_9^l and C_{10}^l are almost flavor universal and the sizes are estimated as $(C_9^l)_{\text{SM}} \simeq -(C_{10}^l)_{\text{SM}} \simeq 4$ at the bottom quark mass scale. There is an ambiguity in the long-distance contribution [7], which is expected to be $\mathcal{O}(\Lambda_{QCD}/m_b)$, but the excesses seem to require much larger contributions to C_9^l and C_{10}^l : $(\Delta C_9^l)/(C_9^l)_{\text{SM}} \simeq -0.2$ and $(\Delta C_{10}^l)/(C_{10}^l)_{\text{SM}} \simeq 0.2$, according to the global fitting [8–17]. Here, $\Delta C_{9,10}^l$ denote the new physics contributions for $C_{9,10}^l$, respectively.

Many new physics scenarios have been proposed in order to explain these $b \rightarrow sll$ anomalies. One simple way is to introduce an extra gauged flavor symmetry [18]. In such a model, the non-vanishing charges are assigned to both μ and quarks and the extra gauge boson contributes to $\Delta C_{9,10}^l$ at the tree-level. Although the B_s meson mixing strongly constrains the contributions, the large $\Delta C_{9,10}^l$ can be achieved successfully if the charge of μ is not vanishing in the mass base. Another candidate for these excesses is namely *leptoquark* that is a scalar or vector field charged under $SU(3)_c$ [19]. The new field couples both leptons and quarks, so that the tree-level exchanging can generate $\Delta C_{9,10}^l$.

We can discuss the other possibility that the large $\Delta C_{9,10}^l$ is realized by the one-loop diagrams involving extra fields [14, 20–25]. For instance, extra vector-like quarks and leptons can be introduced without suffering from gauge anomaly. Further, Yukawa couplings

between the SM fermions and the extra fields can be written down by introducing extra scalar fields.

There are several variations of the extra fields as discussed in Refs. [20, 21]. In all cases, $\mathcal{O}(1)$ Yukawa couplings of μ and extra leptons are required, while moderately small Yukawa couplings of quarks and extra quarks are necessary to realize large enough $\Delta C_{9,10}^l$ but to evade from the stringent bound on the B_s meson mixing. The masses of the extra fields can not be so large to explain such large $\Delta C_{9,10}^l$: the masses of the extra fields should be in the range between $\mathcal{O}(100)$ GeV and $\mathcal{O}(1)$ TeV. Thus it is inevitable to investigate the consistency of the setup with the other observables, such as the direct signals at the LHC and the other flavor violating processes.

It is very interesting that the neutral fields among the extra fermions and scalars become good dark matter (DM) candidates [20–22]. The mass region favored by the excesses corresponds to the one discussed in the Weakly Interacting Massive Particle (WIMP) DM scenario. The size of the interaction with the SM fermions via the Yukawa couplings would not be too large to achieve the DM relic density via the well-known thermal process [22, 26, 27]. As pointed out in Ref. [26], however, this kind of model faces the stringent constraint from the direct-detection experiments of DM. The cross sections are almost on the upper bound of the latest LUX and XENON1T experiments [28–30] if the observed DM relic density is explained by the thermal process. The scattering processes are induced by the photon and Z-boson exchanging at the one-loop level, and the contributions cancel each other in some parameter region. In addition, the tree-level diagrams involving the extra fermions become sizable depending on the alignment of the Yukawa couplings. Moreover, the direct searches for extra quarks and leptons at the LHC are well developed recently. Therefore, the careful integrated study is required to discuss the excesses at the LHCb in this kind of model.

Accordingly, we especially study the DM physics and the LHC physics in this extended model with extra fermions and scalars which couple to both quarks and leptons. The rest of this paper is organized as follows. We introduce our setup in Sec. 2, motivated by the $b \rightarrow sll$ anomalies. We discuss direct searches for extra fermions at the LHC in Sec. 3 and flavor phenomenology in Sec. 4. Then we discuss impacts on DM physics from the other observations, especially the $b \rightarrow sll$ anomalies in Sec. 5. Based on the study of the DM and the LHC physics, we could obtain the upper limits on $\Delta C_{9,10}^l$. We conclude our discussion in Sec. 6.

2 Setup

First of all, we introduce our model motivated by the $b \rightarrow sll$ anomalies at the LHCb experiment. We introduce an extra $SU(2)_L$ -doublet quark, denoted by Q' , and an extra $SU(2)_L$ -doublet lepton, denoted by L' , to enhance C_9^l and C_{10}^l . Their SM charges are summarized in Table 1. We assign global $U(1)_X$ charges to Q' and L' to distinguish them from the SM quarks and leptons. Note that all of the SM particles are neutral under the $U(1)_X$. We also introduce a complex scalar X as a candidate for DM. The DM X

Fields	spin	SU(3) _c	SU(2) _L	U(1) _Y	U(1) _X
Q'	1/2	3	2	1/6	1
L'	1/2	1	2	-1/2	1
X	0	1	1	0	-1

Table 1: Extra fields in our model with global U(1)_X.

is charged under the global U(1)_X symmetry, and it becomes stable if X is lighter than both Q' and L' . The charge assignment of X is shown in Table 1. Note that L' consists of charged and neutral fermions, and the neutral component possibly becomes a good DM candidate. We concentrate on the case that X is DM in this paper.

We can write down the potential for the fermions and the scalar:

$$V = V_F + V_S, \quad (2)$$

$$V_F = m_{Q'} \overline{Q}'_L Q'_R + m_{L'} \overline{L}'_L L'_R + \lambda_i^q \overline{Q}'_R X^\dagger Q_L^i + \lambda_i^l \overline{L}'_R X^\dagger l_L^i + h.c., \quad (3)$$

$$V_S = m_X^2 |X|^2 + \lambda_H |X|^2 |H|^2 + \lambda_X |X|^4 - m_H^2 |H|^2 + \lambda |H|^4. \quad (4)$$

In our notation, (Q^1, Q^2, Q^3) correspond to $((V_{1j}^\dagger u_L^j, d_L)^T, (V_{2j}^\dagger u_L^j, s_L)^T, (V_{3j}^\dagger u_L^j, b_L)^T)$. V_{ij} denotes the CKM matrix. The charged components of (l_L^1, l_L^2, l_L^3) correspond to (e_L, μ_L, τ_L) , respectively. Each SM fermion in Q^i and l_L^i is the mass eigenstate. λ_i^q and λ_i^l is the Yukawa coupling between the DM and the extra fermions. The SM down-type quarks in Q^i and the charged leptons in l_L^i are the mass eigenstates, then we simply denote the Yukawa couplings as $(\lambda_1^q, \lambda_2^q, \lambda_3^q) \equiv (\lambda_d, \lambda_s, \lambda_b)$ and $(\lambda_1^l, \lambda_2^l, \lambda_3^l) \equiv (\lambda_e, \lambda_\mu, \lambda_\tau)$. Note that the scalar potential V_S includes the SM Higgs boson, denoted by H . There are many possibilities of the SM charges and spins of the extra fields. If X is charged under the electroweak symmetry as discussed in Refs. [20, 21], Z -boson exchanging diagram would lead too large cross section for the direct detection of DM. In the case that X is fermion and Q', L' are scalars, the relic density is drastically reduced because of the s -wave contribution. Then, large Yukawa couplings, which are favored by the LHCb excesses, would predict too small relic DM abundance thermally. The fermionic X is, moreover, strongly constrained by the indirect detection of DM.

Based on this setup summarized in Table 1 and Eqs. (2)-(4), we study phenomenology in the LHC, flavor and DM experiments. First, we discuss constraints on these extra fermions and DM from the direct searches at the the LHC in Sec. 3. Then, we investigate the flavor physics and the correlation between the $b \rightarrow sll$ anomalies and the DM physics in Sec. 4 and Sec. 5, respectively.

3 Constraint from the direct search at the LHC

The extra particles summarized in Table 1 could be directly discovered at the LHC. The extra fermion decays to a SM-singlet X and a SM fermion via the Yukawa couplings. The branching ratio of the extra fermion depends on the alignment of the Yukawa couplings. Motivated by the $b \rightarrow sll$ anomalies, we assume $|\lambda_\mu| \gg |\lambda_{e,\tau}|$, and then the extra charged lepton dominantly decays to a singlet and a muon. The expected signal events have two energetic muons and large missing energy, $\mu\mu + E_T^{\text{miss}}$. Note that the neutral extra lepton decays to a singlet and a neutrino, and the decay is totally invisible.

The extra up-type (down-type) quark decays to a singlet and a SM up-type (down-type) quark depending on the Yukawa couplings. If λ_d is relatively large, the contribution of the extra quark exchanging diagram via the Yukawa coupling becomes too large to evade the strong bound from the DM direct detection experiments. On the other hand, the anomalies reported by the LHCb collaboration require sizable $|\lambda_s\lambda_b|$, as discussed in Sec. 4. Therefore, we assume $|\lambda_s\lambda_b| = 0.15$, that corresponds to the upper bound from the $B_s\text{-}\overline{B}_s$ mixing (see Sec. 4), and consider two cases,

$$\begin{aligned} \text{(A)} \quad & \lambda_b = 1.0, \lambda_s = 0.15, \\ \text{(B)} \quad & \lambda_b = \lambda_s = \sqrt{0.15}. \end{aligned}$$

In both cases, λ_d is assumed to be negligibly small. In the case (A), we expect that the extra quark dominantly decays to a singlet and a third-generation quark, and the expected signals are $tt + E_T^{\text{miss}}$ or $bb + E_T^{\text{miss}}$. While the extra quark decays into both a third-generation quark or a second-generation quark with a almost same probability in the case (B).

Since any extra fermions decay to a singlet and produce large missing energies, the extra fermions give similar signals to supersymmetric particles. We refer to the LHC results obtained in the analysis searching for charginos [31] to constrain the extra leptons. For the extra quarks, we refer to the experimental limits from $bb + E_T^{\text{miss}}$ [32] and $jj + E_T^{\text{miss}}$ [33] channels. We do not consider limits from $tt + E_T^{\text{miss}}$ searches because the limits will be weaker than the limit from $bb + E_T^{\text{miss}}$. The mono-jet search is also not important one in our model if the singlet X is the DM. This is because the direct detection easily excludes mass degenerate region where the mono-jet search becomes potentially important, as discussed in Sec. 5.

We calculate the expected number of signals in each signal region using MadGraph5 [34]. The UFO format [35] model files are created by FeynRules [36]. The signal processes are generated from matrix elements with up to an extra parton, then these are passed to PYTHIA 6 [37] for decaying top quarks, parton showering and hadronization. The MLM scheme [38] is used to match the matrix element and parton showering. The generated events are interfaced to DELPHES3 [39] for fast detector simulation. The generated hadrons are clustered using the anti- k_T algorithm [40] with the radius parameter $\Delta R = 0.4$. We basically use the ATLAS DELPHES card, but efficiency formulas of muon reconstruction and b-tagging are changed based on Ref. [41] and Ref. [42]. The muon reconstruction efficiency is set to 0.7 ($|\eta| < 0.1$), 0.99 ($0.1 < |\eta| < 2.5$) and the b-tagging

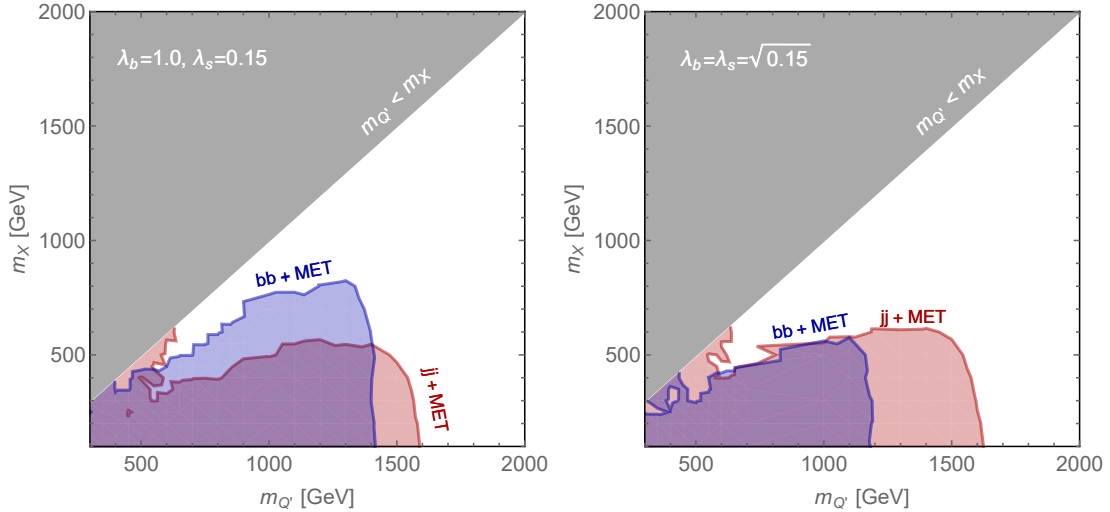


Figure 1: LHC bound for case(A) (left) and case (B) (right). The red regions are excluded by the $jj + E_T^{\text{miss}}$ search and the blue regions are excluded by the $bb + E_T^{\text{miss}}$ search.

efficiency obeys $1.3 \tanh(0.002p_T)30/(1 + 0.086p_T)$, where η , p_T are pseudorapidity and transverse momentum of a jet, respectively. The generated events are normalized according to their cross sections obtained by the event generation and the integrated luminosity of the data: 36.1 fb^{-1} for $bb + E_T^{\text{miss}}$ and $jj + E_T^{\text{miss}}$ searches, and 13.3 fb^{-1} for $ll + E_T^{\text{miss}}$ search.

Figure 1 shows exclusion limits on the extra quarks from the latest searches for $bb + E_T^{\text{miss}}$ (blue) and $jj + E_T^{\text{miss}}$ (red) events. We see in the case (A) that the $jj + E_T^{\text{miss}}$ search is sensitive to heavy extra quark region with the light singlet while the $bb + E_T^{\text{miss}}$ search is more sensitive to the heavier singlet region. In the case (B), the limits from $bb + E_T^{\text{miss}}$ is significantly weakened, while that from $jj + E_T^{\text{miss}}$ is slightly tightened especially in large m_X region.

We refer to the upper bounds on the number of events in the signal regions defined in the $jj + E_T^{\text{miss}}$ search, that require more than two energetic jets and large effective mass, defined as a sum of E_T^{miss} and p_T of jets with $p_T > 50 \text{ GeV}$. Even events with hadronically decaying top quarks can contribute to these signal regions although the produced jets tend to be softer than the ones in the cases that the extra quarks decay to the light quarks directly. Since half of the up-type extra quark decays to a charm quark in the case (B), the limit is slightly tightened compared with the case (A).

The $bb + E_T^{\text{miss}}$ search is dedicated to exotic particles that decay to a bottom quark and a invisible particle exclusively, and the definitions for the signal regions require that there are 2 b-tagged jets and p_T of the fourth jet, ordered in p_T , is smaller than 50 GeV if it exists in an event. These cuts reject the events unless both of the extra quarks decay to a bottom quark. This fact indicates that the branching fraction of the down-type extra quark influences limits from the $bb + E_T^{\text{miss}}$ search significantly. We also found that the t-channel X exchanging production process induced by the large Yukawa coupling is not

$m_d(2 \text{ GeV})$	$4.8^{+0.5}_{-0.3} \text{ MeV}$ [47]	λ	$0.22509^{+0.00029}_{-0.00028}$ [48]
$m_s(2 \text{ GeV})$	$95 \pm 5 \text{ MeV}$ [47]	A	$0.8250^{+0.0071}_{-0.0111}$ [48]
$m_b(m_b)$	$4.18 \pm 0.03 \text{ GeV}$ [47]	$\bar{\rho}$	$0.1598^{+0.0076}_{-0.0072}$ [48]
$\frac{2m_s}{(m_u+m_d)}(2 \text{ GeV})$	27.5 ± 1.0 [47]	$\bar{\eta}$	$0.3499^{+0.0063}_{-0.0061}$ [48]
$m_c(m_c)$	$1.275 \pm 0.025 \text{ GeV}$ [47]	M_Z	$91.1876(21) \text{ GeV}$ [47]
$m_t(m_t)$	$160^{+5}_{-4} \text{ GeV}$ [47]	M_W	$80.385(15) \text{ GeV}$ [47]
α	$1/137.036$ [47]	G_F	$1.1663787(6) \times 10^{-5} \text{ GeV}^{-2}$ [47]
$\alpha_s(M_Z)$	$0.1193(16)$ [47]		

Table 2: The input parameters in our analysis. The CKM matrix, V , is written in terms of λ , A , $\bar{\rho}$ and $\bar{\eta}$ [47].

important and the production process is governed by the usual QCD processes.

We also evaluate limits on the extra leptons from the $ll + E_T^{\text{miss}}$ search, and the result will be shown in Fig. 3. The extra lepton lighter than 500 GeV has already been excluded if the DM is lighter than 300 GeV. This bound is almost independent of the Yukawa coupling and the extra leptons are produced by the Drell-Yan process.

4 Flavor physics

Based on the study in Sec. 3, we investigate the flavor physics especially concerned with the $b \rightarrow sll$ processes, where the LHCb collaboration has reported the deviations from the SM predictions. In our model, the $b \rightarrow s$ transition is induced by the box diagram involving Q' , L' and X . We notice that the operator relevant to the B_s - \bar{B}_s mixing is also generated by the similar box diagram involving Q' and X . In this section, we discuss not only the rare B decay, but also the other flavor processes relevant to our scenario.

4.1 Constraints from the B_s - \bar{B}_s mixing

In Refs. [26, 43], the contributions to $\Delta F = 2$ processes have been studied in this kind of model. Now, we are especially interested in the B_s - \bar{B}_s mixing, since that process directly relates to the $b \rightarrow s$ transition. The box diagram involving X and Q' induces the operators relevant to the B_s - \bar{B}_s mixing:

$$\mathcal{H}_{eff}^{\Delta F=2} = (C_1)_{sb} (\bar{s}_L \gamma^\mu b_L) (\bar{s}_L \gamma^\mu b_L) + h.c.. \quad (5)$$

The Wilson coefficient at the one-loop level is given by [26],

$$(C_1)_{sb} = \frac{(\lambda_b \lambda_s^*)^2}{64\pi^2} \frac{1}{(m_{Q'}^2 - m_X^2)^2} \left\{ \frac{m_{Q'}^2 + m_X^2}{2} + \frac{m_X^2 m_{Q'}^2}{m_{Q'}^2 - m_X^2} \ln \left(\frac{m_X^2}{m_{Q'}^2} \right) \right\}. \quad (6)$$

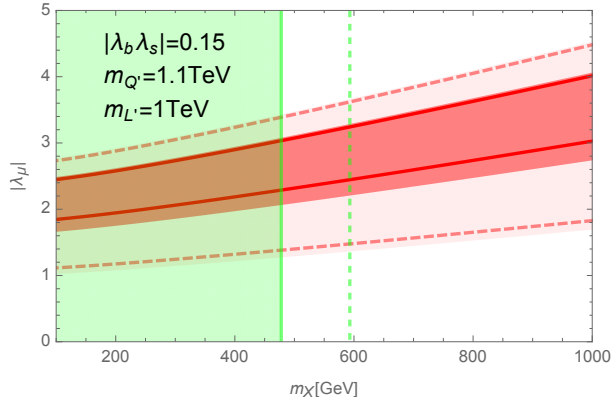


Figure 2: The required values of λ_μ for the R_K and R_{K^*} anomalies when $m_{L'} = 1$ TeV, $|\lambda_b \lambda_s| = 0.15$ and $m_{Q'} = 1.1$ TeV. The (light) red region is the 1σ (2σ) region of R_K . The region for R_{K^*} is not so different from the R_K . The bands within thick and dashed red lines correspond to 1σ and 2σ regions of R_{K^*} . The (dashed) green line depicts the lower limit from B_s - \overline{B}_s mixing in Eq. (7) at $m_{Q'} = 1.1$ TeV (1 TeV).

One important observable of the B_s - \overline{B}_s mixing is the mass difference, Δm_s , that is measured with high accuracy: $\Delta m_s = 17.757 \pm 0.021$ ps $^{-1}$ [44]. The SM prediction, however, still suffers from the large uncertainty of the form factor: $f_{B_s} \hat{B}_{B_s}^{1/2} = 0.266 \pm 0.018$ [45], where f_{B_s} is the decay constant of the B_s meson and \hat{B}_{B_s} is the bag parameter. We obtain the SM prediction as $(\Delta m_s)_{\text{SM}} = 18.358$ ps $^{-1}$, using $m_{B_s} = 5.3663$ GeV and $\eta_B = 0.55$ [46]. The input parameters used in our analysis are summarized in Table 2. Taking into account the error, the SM prediction is consistent with the experimental result. Therefore, we estimate the upper limit of the deviation from the SM prediction within 1σ and draw the bound on the parameters in this model.

The upper bound on the deviation from the SM prediction is estimated as about 14 %. When $|\lambda_b \lambda_s|$ is fixed at 0.15, the lower bound on the DM mass is estimated as follows:

$$m_X \geq 593 \text{ GeV (478 GeV)}, \quad (7)$$

at $m_{Q'} = 1$ TeV (1.1 TeV).

4.2 The excesses of the $b \rightarrow s ll$ processes

Finally, we consider the $b \rightarrow s ll$ ($l = e, \mu$) decays. The explanation of the anomaly has been done in the setups similar to our model [20,21]. In our setup, the box diagram, that involves X , Q' and L' , contributes to the flavor violating processes, $b \rightarrow s ll$. The $\Delta B = 1$ effective Hamiltonian is given by

$$\mathcal{H}_{\text{eff}} = -g_{\text{SM}} \{ C_9^l (\overline{s_L} \gamma_\mu b_L) (\overline{l} \gamma^\mu l) + C_{10}^l (\overline{s_L} \gamma_\mu b_L) (\overline{l} \gamma^\mu \gamma_5 l) + h.c. \}, \quad (8)$$

where g_{SM} is the factor from the SM contribution:

$$g_{\text{SM}} = \frac{4G_F}{\sqrt{2}} V_{tb} V_{ts}^* \frac{e^2}{16\pi^2}. \quad (9)$$

The Wilson coefficients C_9^l and C_{10}^l consist of the SM and the new physics contributions as $C_9^l = (C_9^l)_{\text{SM}} + \Delta C_9^l$ and $C_{10}^l = (C_{10}^l)_{\text{SM}} + \Delta C_{10}^l$. The new physics contributions in this model are given by

$$\Delta C_9^\mu = -\Delta C_{10}^\mu = \frac{\lambda_b \lambda_s^* |\lambda_\mu|^2}{128\pi^2 g_{\text{SM}}} \frac{1}{m_{Q'}^2 - m_{L'}^2} \{f(m_X^2/m_{Q'}^2) - f(m_X^2/m_{L'}^2)\}, \quad (10)$$

where $f(x)$ is defined as

$$f(x) = \frac{1}{x-1} - \frac{\ln x}{(x-1)^2}. \quad (11)$$

The branching fractions $\text{BR}(B^+ \rightarrow K^+ ll)$ and $\text{BR}(B_0 \rightarrow K^* ll)$ are recently measured in the LHCb experiment [1, 2]. In the SM, the ratio between the branching fractions for $l = \mu$ and $l = e$ is predicted to be almost unity. The measured values of such observables, namely R_K and R_{K^*} , are reported in each bin of q^2 GeV², which is the invariant mass of two leptons in the final state [1, 2]. In particular, both results in $B^+ \rightarrow K^+ \mu\mu$ and $B_0 \rightarrow K^* \mu\mu$ with $1 \text{ GeV}^2 \leq q^2 \leq 6 \text{ GeV}^2$ are smaller than the SM predictions, and the deviations of R_K and R_{K^*} exceed 2σ : $R_K = 0.745 \pm 0.097$ [1] and $R_{K^*} = 0.685 \pm 0.122$ [2]. In the region with lower q^2 , we can also see the deviation of R_{K^*} , although the contribution from the electric dipole operator needs to be taken into account [2].

As discussed in Refs. [8–17], the new physics contributions to C_9^l and C_{10}^l are required to explain the excesses. R_K and R_{K^*} including the new physics contributions, for instance, are calculated in Refs. [10, 49, 50].

Figure 2 shows the required values of λ_μ for the R_K and R_{K^*} anomalies when $m_{L'} = 1 \text{ TeV}$, $|\lambda_b \lambda_s| = 0.15$ and $m_{Q'} = 1.1 \text{ TeV}$. The (light) red region is the 1σ (2σ) region of R_K . The bands within thick and dashed red lines correspond to 1σ and 2σ regions of R_{K^*} . The (dashed) green line depicts the lower limit from the $B_s\text{-}\overline{B}_s$ mixing in Eq. (7) at $m_{Q'} = 1.1 \text{ TeV}$ (1 TeV). We see that λ_μ need to be about 2 to explain the excesses within 1σ .

In Fig. 3, the predicted ΔC_9^l is also depicted on the $m_{L'}\text{-}m_X$ plane, when λ_μ is fixed at $\lambda_\mu = 2$. The value required by the global fitting, where the angular distribution of $B \rightarrow K^* \mu\mu$ is also included, is about 25 %, compared to the SM prediction. The magnitudes of $(C_9^l)_{\text{SM}}$ and $(C_{10}^l)_{\text{SM}}$ are about 4, so that $\mathcal{O}(1)$ value of $|\Delta C_9^\mu|$ seems to be required by the global analysis. As we see in Fig. 3, the region with $|\Delta C_9^\mu| \gtrsim 0.5$ is below the exclusion limit from the $B_s\text{-}\overline{B}_s$ mixing. The 1σ region of $|\Delta C_9^\mu|$ suggested by the global analysis, for instance, is $-0.81 \leq \Delta C_9^\mu \leq -0.48$ (1σ) and $-1.00 \leq \Delta C_9^\mu \leq -0.32$ (2σ) [13]. Then, we could conclude that our model can fit the experimental results including the angular distribution of $B \rightarrow K^* \mu\mu$ within 2σ but not 1σ as far as λ_μ is equal to 2.

In the next section, we study DM physics based on these analyses. In this kind of model, large Yukawa couplings are required by the thermal relic density, because the

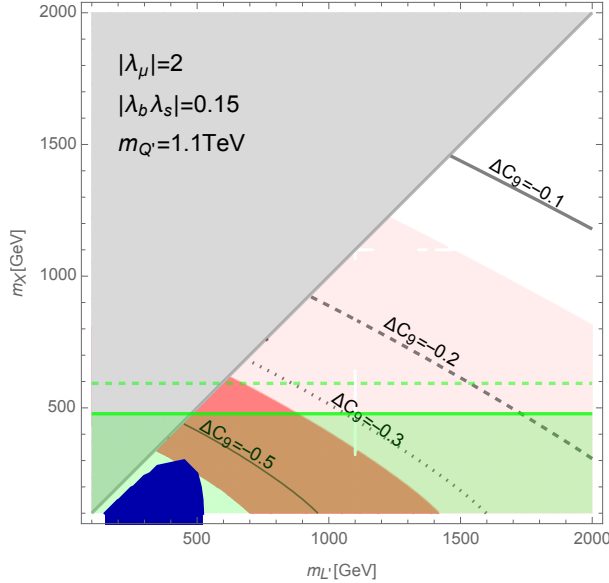


Figure 3: ΔC_9 on the plane of $m_{L'}$ and m_X with $|\lambda_\mu| = 2$, $|\lambda_b \lambda_s| = 0.15$ and $m_{Q'} = 1.1$ TeV. The size of $\Delta C_9 = -\Delta C_{10}$ on each black line is -0.1 (thick), -0.2 (dashed), -0.3 (dotted), and -0.5 (solid), respectively. The (light) red region is the 1σ (2σ) region of R_K . The (dashed) green line depicts the lower limit from $B_s - \bar{B}_s$ mixing in Eq. (7) at $m_{Q'} = 1.1$ TeV (1 TeV). The blue region is excluded by $\mu\mu + E_T^{\text{miss}}$ at the LHC [31].

DM candidate is a complex scalar. Then, we will find the parameter region that the explanation of the excesses within 2σ as well as the DM relic density can be achieved.

Before the DM physics, let us discuss the other observables in flavor physics. We simply assume that λ_d is tiny to avoid the strong constraints from $K_0 - \bar{K}_0$ and $B_d - \bar{B}_d$ mixings. In this setup, since $SU(2)_L$ doublet quarks couple to the extra quarks and DM, the sizable λ_b and λ_s generate sizable Yukawa couplings between left-handed up-type quarks and the extra up-type quarks as well. Then, the constraint from $D_0 - \bar{D}_0$ should be taken into account. The relevant Yukawa couplings are as follows:

$$(\lambda_s V_{us}^* + \lambda_b V_{ub}^*) \overline{Q'_{1R}} X^\dagger u_L + (\lambda_s V_{cs}^* + \lambda_b V_{cb}^*) \overline{Q'_{1R}} X^\dagger c_L. \quad (12)$$

Here, Q'_1 denotes the isospin 1/2 component of Q' . Each coupling is suppressed by the CKM matrix, and the most relevant coupling is expected to be induced by λ_s because of the relatively large elements of the CKM matrix.

On the other hand, the theoretical prediction of $D_0 - \bar{D}_0$ also suffers from the ambiguity of the long-distance correction [51, 52]. Therefore, we estimate the new physics contributions and compare the order of the SM prediction. The Yukawa couplings in Eq. (12) induce the $\Delta F = 2$ operator with $(C_1)_{uc}$ via the box diagram. The observable of the $D_0 - \bar{D}_0$ mixing is given by

$$x_D = 2 |M_{12}^D| \tau_D, \quad (13)$$

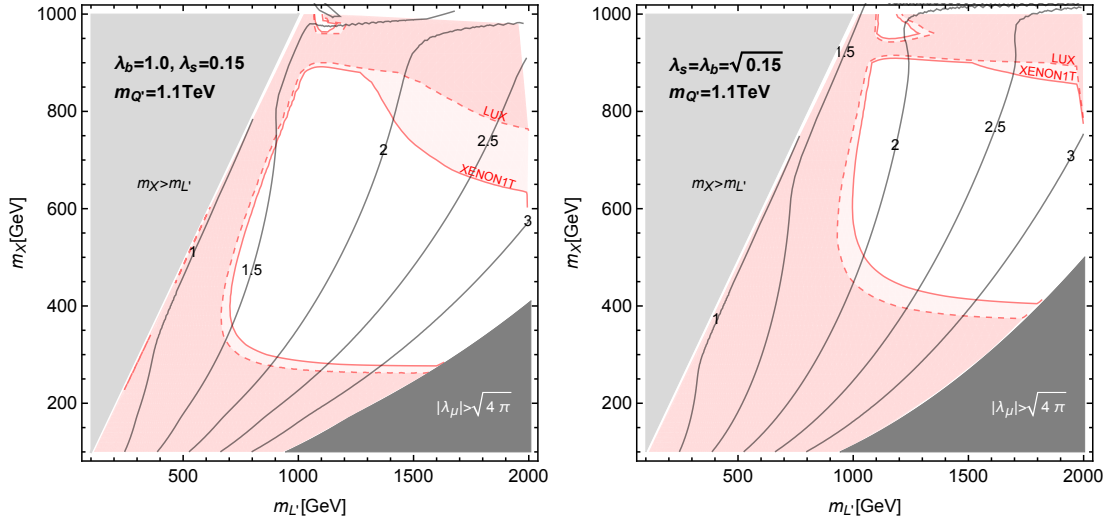


Figure 4: The values of $|\lambda_\mu|$ required for the central value of the observed DM abundance (black solid lines); $\Omega_{\text{CDM}} h^2 = 0.1186 \pm 0.0020$ [47]. The left (right) panel corresponds to the case A (case B). DM direct detection experiments constrain the red region.

where τ_D is the life time: $\tau_D = 0.41$ ps [47]. M_{12}^D includes both the SM prediction and the new physics contribution. Using the input parameters in Refs. [47, 53, 54], the new physics contribution to x_D is estimated as $\sim 2 \times 10^{-4}$ at $(\lambda_b, \lambda_s) = (1, 0.15)$, $m_{Q'} = 1$ TeV and $m_X = 500$ GeV. The SM prediction is $\mathcal{O}(10^{-2})$ [52], so that these parameters are safe for the D_0 - \bar{D}_0 mixing. The upper bound on λ_s would be about 0.3. If λ_s is $\mathcal{O}(1)$ and λ_b is $\mathcal{O}(0.1)$, the new physics contribution becomes hundreds times bigger than the SM prediction. Thus, we concentrate on the case (A) and the case (B) where $|\lambda_b| \geq |\lambda_s|$ is satisfied.

5 The impact on DM physics

Here, we study DM physics and discuss the consistency between the explanation of the $b \rightarrow sll$ anomalies and the DM observations. As discussed above, the $b \rightarrow sll$ anomalies and the constraints from the $\Delta F = 2$ processes imply that $|\lambda_b \lambda_s| = 0.15$ and $|\lambda_b| \geq |\lambda_s|$ for $m_{Q'} = 1.1$ TeV. Then, in this section, we analyze the DM relic density and the direct detection bounds, focusing on two parameter sets: $(\lambda_b, \lambda_s) = (1.0, 0.15)$ (Case A) and $(\lambda_b, \lambda_s) = (\sqrt{0.15}, \sqrt{0.15})$ (Case B). In both cases, $m_{Q'}$ is fixed at 1.1 TeV. Note that we employ micrOMEGAs_4.3.4 [55] to evaluate the DM relic density in our analysis.

5.1 Relic density

The DM annihilation process is governed by the extra quark and lepton exchanging in t -channel: $XX^\dagger \rightarrow Q\bar{Q}, \bar{l}l$. Since the Yukawa terms in Eq.(3) preserve the chiralities of

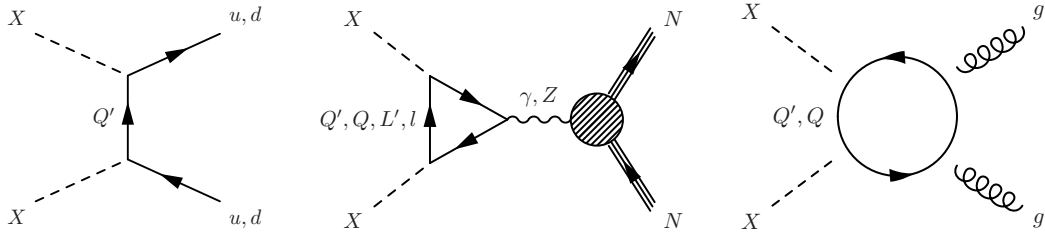


Figure 5: Diagrams contributing to the DM-nucleon elastic scattering.

the interacting fermions, the final state fermions are left-handed in the massless limit. Then, the s -wave contribution is suppressed by the fermion mass, so that the annihilation becomes p -wave dominant. That requires the Yukawa coupling to be so large that the observed value of the DM abundance is explained thermally. As seen in Fig. 2, the $b \rightarrow sll$ anomalies also require a large $|\lambda_\mu|$, and this fact indicates that the $b \rightarrow sll$ anomalies can be compatible with the observed DM density in our model.

In Fig. 4, we show the values of $|\lambda_\mu|$, by black lines, required to explain the central value of the observed DM abundance: $\Omega_{\text{CDM}}h^2 = 0.1186 \pm 0.0020$ [47]. In the case (B) with $|\lambda_b| = |\lambda_s| = \sqrt{0.15}$, the dominant annihilation process is $XX^\dagger \rightarrow \mu\bar{\mu}, \nu\bar{\nu}$ in our parameter space, except for the coannihilation region. We find in the right panel of Fig. 4 that $|\lambda_\mu| \simeq 2$ is predicted by $(m_X, m_{L'}) = (500 \text{ GeV}, 1 \text{ TeV})$. The $b \rightarrow sll$ anomalies are simultaneously explained with the DM density around this region.

In the case (A) with $|\lambda_b| = 1.0$ and $|\lambda_s| = 0.15$, other processes, especially $XX^\dagger \rightarrow b\bar{b}, t\bar{t}$, may assist in reducing the DM relic density in addition to $XX^\dagger \rightarrow \mu\bar{\mu}, \nu\bar{\nu}$. Since we fix $m_{Q'}$ at 1.1 TeV, these processes dominate the annihilation process in the region with $m_{L'} > 1 \text{ TeV}$. In fact, we find in the left panel of Fig. 4 that the observed density is explained by smaller values of $|\lambda_\mu|$ than the case (B).

5.2 Direct detection

Next, we discuss the constraint from the DM direct detection. Figure 5 shows relevant processes to the DM-nucleon scattering in this model. The type of dominant process depends on mass spectrum of the DM and the extra fermion and the size of the Yukawa couplings.

If the DM has a sizable interaction with the up or down quarks, the dominant contribution to the direct detection will be the tree-level scattering through the extra quark exchanging, as the left diagram in Fig. 5. This process is not suppressed by nucleon form factors, and thus leads a large cross section. Note that in our model, even if λ_d is vanishing, the DM can interact with the up quark through the CKM matrix as in Eq.(12).

There are large contributions from the 1-loop vector-boson exchanging, as shown in the center of Fig. 5, because the large Yukawa coupling is required by the DM relic density. As studied in the literatures [26, 27, 56], the triangle diagram involving the SM fermion f and the extra fermion F induces the scattering of DM with the proton through the

photon exchanging, and the contribution is given by

$$f_p^{\text{photon}} \simeq \frac{e^2 Q_f |\lambda_f|^2 N_c}{16\pi^2 m_F^2} \frac{N_c}{3} \ln \left(\frac{m_f^2}{m_F^2} \right), \quad (14)$$

in the limit that $m_F \gg m_X, m_f$. N_c and Q_f denote the number of color and the electromagnetic charge for the fermion f . It is interesting that there is a logarithm enhancement as $\ln(m_f^2/m_F^2)$, so that the lighter fermion has larger contribution.

In addition, the diagram similar to the photon exchanging also generates the Z -boson exchanging process. The contribution is evaluated as

$$f_p^Z = (4s_W^2 - 1) \frac{G_F a_Z}{\sqrt{2}}, \quad f_n^Z = \frac{G_F a_Z}{\sqrt{2}}, \quad (15)$$

where s_W denotes the sine of the Weinberg angle and a_Z is a loop function:

$$a_Z \simeq \frac{T_3^f N_c |\lambda_f|^2 m_f^2}{16\pi^2 m_F^2} \left[\frac{3}{2} + \ln \left(\frac{m_f^2}{m_F^2} \right) \right], \quad (16)$$

with T_3^f being isospin of the SM fermion f in the loop. Since the Z -exchanging contribution is proportional to m_f^2/m_F^2 , this process is significant in the case that f is the top quark. In our analysis, we use exact expressions for these vector-boson exchanging contributions, not the approximate forms, Eqs.(14) and (16).

Besides, DM can also scatter off the gluon in the nucleon through the box diagram involving the heavy and extra quarks, depicted as the right piece of Fig. 5. This contribution is less than 10% of the photon exchanging contribution in most of our parameter space, as discussed in Ref [26]. However, this process is largely enhanced to be dominant contribution in the region of $m_{Q'} - m_X \simeq m_q$ [57–59]. This contribution is included in our analysis by using micrOMEGAs.

In the case (B) with $|\lambda_b| = |\lambda_s| = \sqrt{0.15}$, the DM significantly interacts with the leptons. The Yukawa interaction involving the lepton does not induce the tree-level process, and the dominant process is the 1-loop photon exchanging in most of our parameter space. On the other hand, λ_s induces the sizable tree-level scattering with the up quark via the CKM mixing. Although λ_s is much smaller than λ_μ , it is possible that λ_s gives sizable contributions to the direct detection. This process becomes dominant in the region where both m_X and $m_{L'}$ are large even when we fix $m_{Q'}$ at 1.1 TeV and much larger than $m_{L'}$. In the right panel of Fig. 6, we find that $400 \text{ GeV} \lesssim m_X \lesssim 900 \text{ GeV}$ and $m_{L'} \gtrsim 1 \text{ TeV}$ are allowed by the XENON1T experiment [30].

In the case (A) of $|\lambda_b| = 1$ and $|\lambda_s| = 0.15$, there is a large contribution from the Z -boson exchanging via the top-quark loop, in addition to the photon exchanging. Even in this case, the photon exchanging is dominant process in the smaller mass region. The Z -boson exchanging dominates the DM-nucleon scattering in $m_X \gtrsim 400 \text{ GeV}$ and $m_{L'} \gtrsim 1 \text{ TeV}$, except for the region where $m_{Q'} - m_X \simeq m_t$ and the gluon scattering is dominant. Moreover, we emphasize that the photon and Z -boson exchanging are comparable and the sign is opposite. Thus there is a considerable cancellation between them. In the left panel of Fig. 6, we find that the allowed DM mass is $300 \text{ GeV} \lesssim m_X \lesssim 900 \text{ GeV}$ to evade the XENON1T bound [30].

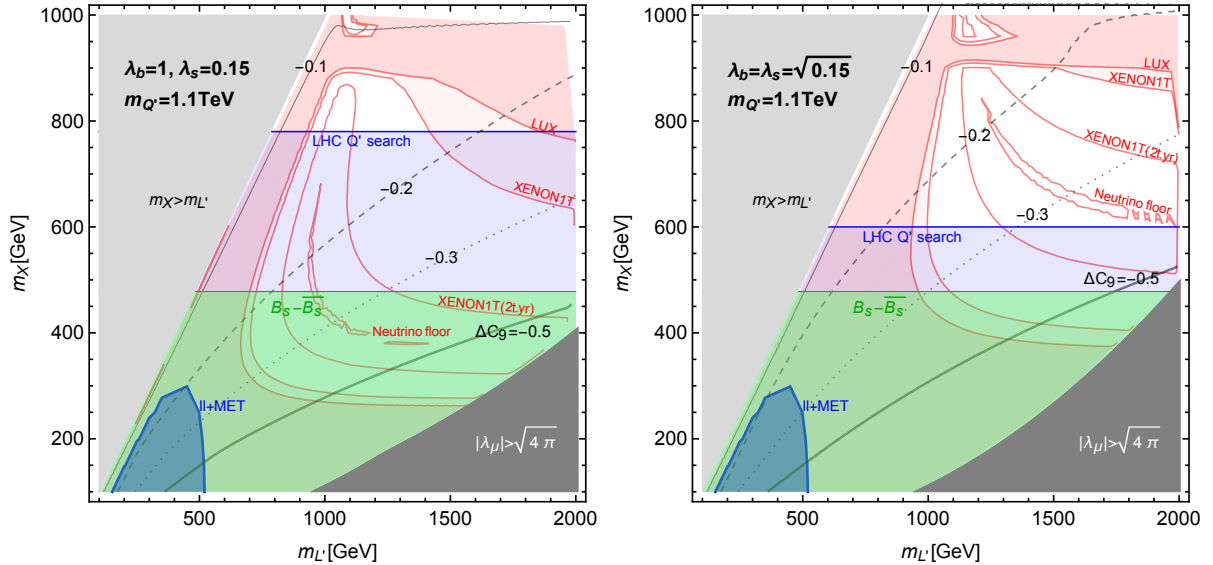


Figure 6: The ΔC_9^μ value (black lines), when the value of $|\lambda_\mu|$ is aligned to explain the observed DM abundance. The left (right) panel corresponds to the case A (case B). We fill in the region excluded by the LHC, flavor and DM experiments with colors; the extra quark and lepton searches (blue), $B_s-\bar{B}_s$ mixing (green) and DM direct detection experiments (red). The gray region stands for the perturbativity limit; $|\lambda_\mu| > \sqrt{4\pi}$.

5.3 $b \rightarrow sll$ anomalies with the observed DM abundance

In the Fig. 6, we depict the values of ΔC_9 by black lines, when $|\lambda_\mu|$ is aligned to account for the measured DM density. The left (right) panel corresponds to the case (A) (case (B)). Shaded region is excluded by the LHC, flavor and DM experiments; the extra quark and lepton searches at the LHC (blue), the $B_s-\bar{B}_s$ mixing observables (green) and the DM direct detections (red). We also fill in the region constrained by the theoretical requirement with colors; the perturbative bound $|\lambda_\mu| > \sqrt{4\pi}$ (gray) and the unstable X , $m_X > m_{L'}$ (light gray). Further, we show the future sensitivity prospects in XENON1T experiment and neutrino floor in the figure.

In the case (A) (left panel), we see that the Q' searches at the LHC and the DM direct detection stringently limit our model parameter. Then, the region where $\Delta C_9^\mu \lesssim -0.2$ is excluded by these results. Following Ref. [13], the global fitting of $\Delta C_9^\mu = -\Delta C_{10}^\mu$ suggests $-0.81 \leq \Delta C_9^\mu \leq -0.48$ (1σ) and $-1.00 \leq \Delta C_9^\mu \leq -0.32$ (2σ). Thus, we conclude that it is difficult to explain the $b \rightarrow sll$ anomalies within even 2σ in the case (A).

In the case (B), on the other hand, we find that even the region where $\Delta C_9^\mu \lesssim -0.3$ is allowed and the $b \rightarrow sll$ anomalies can be explained within 2σ , consistently with the other experiments.

6 Summary

The LHCb collaboration has reported several excesses in the $b \rightarrow sll$ processes. A common feature is that the branching ratio of the b decay associated with two muons is rather small, compared to the SM prediction. If the excesses are evidences for new physics, they may indicate existences of flavor-violating couplings between the SM fermions and new particles *. So far, many candidates for the new physics have been proposed: Z' [18], leptoquark [19], and so on. In those models, the tree-level diagram involving the extra particle contributes to C_9 and C_{10} operators. Although we may have to introduce many extra fields especially in Z' models to achieve the realistic Yukawa couplings and the anomaly-free conditions, we can simply explain the excesses without conflicts with the other flavor observables [18, 19].

In this paper, we focus on the other simple scenario that extra fields charged under the SM gauge symmetries are introduced and the one-loop diagram involving the extra fields contributes to the C_9 and C_{10} operators [14, 20–25]. In order to explain the experimental results of $R_K^{(*)}$, we need rather large Yukawa couplings between the extra lepton and muon. The Yukawa couplings in the quark sector, on the other hand, need to be rather small to avoid the constraint from the B_s - \overline{B}_s mixing. An interesting point of this setup is that the EW-neutral scalar can be interpreted as a good DM candidate and such large Yukawa couplings predict a large cross section of DM annihilation moderately to explain the DM relic density. Besides, the cross section of the DM direct detection is predicted to be just below the current experimental upper bound in this kind of model [26]. In our model motivated by the excesses in the LHCb experiment, we have found that the cross section for the DM direct detection has a non-trivial structure: the photon exchanging and Z exchanging diagrams cancel each other in some parameter region. Then, the cross section is estimated as the one just below the current experimental bound [29, 30] in the region with the $\mathcal{O}(1)$ -TeV mass of L' and about 500-GeV mass of the DM. Around the region, the predicted C_9 and C_{10} become large enough to achieve the $R_K^{(*)}$ experimental results within 1σ level. We can expect that the DM direct detection experiments [30] will prove our model if our DM is the dominant component of the relic density.

We can consider the other setups to explain the excesses; for instance, DM is a fermion and extra quarks/leptons are scalar fields. In such a case, large λ_μ , which is favored by the excesses, could not be consistent with the relic density of DM. As studied in Ref. [26], the relic density requires $|\lambda_\mu| \leq 1$, when $m_X = 500$ GeV and $m_{Q'} = m_{L'} = 1$ TeV. In addition, the constraint from the indirect detection of DM excludes $m_X \lesssim 1$ TeV in this fermionic DM case. Thus, the scalar DM scenario seems to be favored from the viewpoint of the consistency between the excesses and the DM observables.

Finally, let us also give a comment on the difference between our setup and the other models that have been studied before. In Refs. [20, 21], the explanation of the excesses has been done using the box diagram involving extra scalars and fermions. The possible EW charge assignments for the extra fields are well summarized, and the model with the DM

*Note that the explanation of the excess without new flavor-violating couplings is also possible [25].

charged under the EW symmetry is discussed in Ref. [20]. In our paper, we concentrate on the case that the DM is neutral under the EW symmetry, and we have carefully studied the dark matter physics and collider physics taking into account the flavor dependence as well. We conclude that both the DM direct detection and the LHC results strictly limit the explanation of the excess even in our model. If the DM is charged under the EW symmetry, as discussed in Ref. [20], the Z -boson exchanging would drastically enhance the DM direct-detection cross section and the bound would become more severe than ours. We assign the global $U(1)_X$ symmetry to stabilize the DM. We can consider the gauge $U(1)_X$ as discussed in Ref. [22]. The authors in Ref. [22] consider the possibility that there is a mass mixing between the extra quark and the SM quarks. Then, the massive $U(1)_X$ gauge boson exchanging explains the excess. In this case, the collider signal of the extra quark is different from ours, so that the model with the gauged $U(1)_X$ may be able to evade the strong bound from the LHC experiment. Even in such a case, however, we emphasize that the DM direct detection cross section plays an important role in testing this kind of model, as far as the DM is complex scalar. In Ref. [22], the real scalar DM scenario is discussed, so that the bound from the DM direct detection could be relaxed, although the Yukawa coupling required by the thermal relic density is larger than the one in our model.

Acknowledgments

The work of J. K. is supported by Grant-in-Aid for Research Fellow of Japan Society for the Promotion of Science No. 16J04215. The work of Y. O. is supported by Grant-in-Aid for Scientific research from the Ministry of Education, Science, Sports, and Culture (MEXT), Japan, No. 17H05404.

References

- [1] R. Aaij *et al.* [LHCb Collaboration], Phys. Rev. Lett. **113**, 151601 (2014) [arXiv:1406.6482 [hep-ex]].
- [2] Talk by Simone Bifina for the LHCb collaboration, CERN, 18/4/2017.
- [3] R. Aaij *et al.* [LHCb Collaboration], JHEP **1509**, 179 (2015) [arXiv:1506.08777 [hep-ex]].
- [4] R. Aaij *et al.* [LHCb Collaboration], JHEP **1506**, 115 (2015) [arXiv:1503.07138 [hep-ex]].
- [5] R. Aaij *et al.* [LHCb Collaboration], Phys. Rev. Lett. **111**, 191801 (2013) [arXiv:1308.1707 [hep-ex]].
- [6] R. Aaij *et al.* [LHCb Collaboration], JHEP **1602**, 104 (2016) [arXiv:1512.04442 [hep-ex]].

- [7] A. Khodjamirian, T. Mannel, A. A. Pivovarov and Y.-M. Wang, JHEP **1009**, 089 (2010) [arXiv:1006.4945 [hep-ph]]; A. Khodjamirian, T. Mannel and Y. M. Wang, JHEP **1302**, 010 (2013) [arXiv:1211.0234 [hep-ph]].
- [8] S. Descotes-Genon, J. Matias and J. Virto, Phys. Rev. D **88**, 074002 (2013) [arXiv:1307.5683 [hep-ph]].
- [9] G. Hiller and M. Schmaltz, Phys. Rev. D **90**, 054014 (2014) [arXiv:1408.1627 [hep-ph]].
- [10] S. Descotes-Genon, L. Hofer, J. Matias and J. Virto, JHEP **1606**, 092 (2016) [arXiv:1510.04239 [hep-ph]].
- [11] W. Altmannshofer and D. M. Straub, arXiv:1503.06199 [hep-ph].
- [12] T. Hurth, F. Mahmoudi and S. Neshatpour, Nucl. Phys. B **909**, 737 (2016) [arXiv:1603.00865 [hep-ph]].
- [13] W. Altmannshofer, P. Stangl and D. M. Straub, arXiv:1704.05435 [hep-ph].
- [14] G. D'Amico, M. Nardecchia, P. Panci, F. Sannino, A. Strumia, R. Torre and A. Urbano, arXiv:1704.05438 [hep-ph].
- [15] L. S. Geng, B. Grinstein, S. Jäger, J. Martin Camalich, X. L. Ren and R. X. Shi, arXiv:1704.05446 [hep-ph].
- [16] M. Ciuchini, A. M. Coutinho, M. Fedele, E. Franco, A. Paul, L. Silvestrini and M. Valli, arXiv:1704.05447 [hep-ph].
- [17] A. K. Alok, D. Kumar, J. Kumar and R. Sharma, arXiv:1704.07347 [hep-ph].
- [18] S. M. Boucenna, A. Celis, J. Fuentes-Martin, A. Vicente and J. Virto, Phys. Lett. B **760**, 214 (2016) [arXiv:1604.03088 [hep-ph]]; S. M. Boucenna, A. Celis, J. Fuentes-Martin, A. Vicente and J. Virto, JHEP **1612**, 059 (2016) [arXiv:1608.01349 [hep-ph]]; Q. Chang, X. Q. Li and Y. D. Yang, JHEP **1004**, 052 (2010) [arXiv:1002.2758 [hep-ph]]; Q. Chang, X. Q. Li and Y. D. Yang, J. Phys. G **41**, 105002 (2014) [arXiv:1312.1302 [hep-ph]]; A. Crivellin, G. D'Ambrosio and J. Heeck, Phys. Rev. D **91**, no. 7, 075006 (2015) [arXiv:1503.03477 [hep-ph]]; W. Altmannshofer and I. Yavin, Phys. Rev. D **92**, no. 7, 075022 (2015) [arXiv:1508.07009 [hep-ph]]; B. Allanach, F. S. Queiroz, A. Strumia and S. Sun, Phys. Rev. D **93**, no. 5, 055045 (2016) [arXiv:1511.07447 [hep-ph]]; I. Garcia Garcia, arXiv:1611.03507 [hep-ph]; P. Ko, T. Nomura and H. Okada, arXiv:1701.05788 [hep-ph]; P. Ko, T. Nomura and H. Okada, arXiv:1702.02699 [hep-ph]; P. Ko, Y. Omura, Y. Shigekami and C. Yu, arXiv:1702.08666 [hep-ph]; Y. Tang and Y. L. Wu, arXiv:1705.05643 [hep-ph]; S. Di Chiara, A. Fowlie, S. Fraser, C. Marzo, L. Marzola, M. Raidal and C. Spethmann, arXiv:1704.06200 [hep-ph]; R. Alonso, P. Cox, C. Han and T. T. Yanagida, arXiv:1704.08158 [hep-ph]; C. Bonilla, T. Modak, R. Srivastava and J. W. F. Valle,

- arXiv:1705.00915 [hep-ph]; J. Ellis, M. Fairbairn and P. Tunney, arXiv:1705.03447 [hep-ph]; R. Alonso, P. Cox, C. Han and T. T. Yanagida, arXiv:1705.03858 [hep-ph]; A. Datta, J. Kumar, J. Liao and D. Marfatia, arXiv:1705.08423 [hep-ph]; C. W. Chiang, X. G. He, J. Tandean and X. B. Yuan, arXiv:1706.02696 [hep-ph]; D. Ghosh, arXiv:1704.06240 [hep-ph]; A. K. Alok, B. Bhattacharya, A. Datta, D. Kumar, J. Kumar and D. London, arXiv:1704.07397 [hep-ph].
- [19] M. Bauer and M. Neubert, Phys. Rev. Lett. **116**, no. 14, 141802 (2016) [arXiv:1511.01900 [hep-ph]]; D. Das, C. Hati, G. Kumar and N. Mahajan, Phys. Rev. D **94**, 055034 (2016) [arXiv:1605.06313 [hep-ph]]; D. Bečirević, S. Fajfer, N. Košnik and O. Sumensari, Phys. Rev. D **94**, no. 11, 115021 (2016) [arXiv:1608.08501 [hep-ph]]; S. Sahoo, R. Mohanta and A. K. Giri, Phys. Rev. D **95**, 035027 (2017) [arXiv:1609.04367 [hep-ph]]; G. Hiller, D. Loose and K. Schonwald, JHEP **1612**, 027 (2016) [arXiv:1609.08895 [hep-ph]]; B. Bhattacharya, A. Datta, J. P. Guevin, D. London and R. Watanabe, JHEP **1701**, 015 (2017) [arXiv:1609.09078 [hep-ph]]; D. Bečirević and O. Sumensari, arXiv:1704.05835 [hep-ph]; Y. Cai, J. Gargalionis, M. A. Schmidt and R. R. Volkas, arXiv:1704.05849 [hep-ph]; D. Das, C. Hati, G. Kumar and N. Mahajan, arXiv:1705.09188 [hep-ph]; A. Crivellin, D. Müller and T. Ota, arXiv:1703.09226 [hep-ph]; S. Matsuzaki, K. Nishiwaki and R. Watanabe, arXiv:1706.01463 [hep-ph]; A. K. Alok, B. Bhattacharya, A. Datta, D. Kumar, J. Kumar and D. London, arXiv:1704.07397 [hep-ph].
- [20] B. Gripaios, M. Nardecchia and S. A. Renner, JHEP **1606**, 083 (2016) [arXiv:1509.05020 [hep-ph]].
- [21] P. Arnan, L. Hofer, F. Mescia and A. Crivellin, JHEP **1704**, 043 (2017) [arXiv:1608.07832 [hep-ph]].
- [22] G. Bélanger, C. Delaunay and S. Westhoff, Phys. Rev. D **92**, 055021 (2015) [arXiv:1507.06660 [hep-ph]].
- [23] Q. Y. Hu, X. Q. Li and Y. D. Yang, Eur. Phys. J. C **77**, no. 3, 190 (2017) [arXiv:1612.08867 [hep-ph]].
- [24] Z. Poh and S. Raby, arXiv:1705.07007 [hep-ph].
- [25] J. F. Kamenik, Y. Soreq and J. Zupan, arXiv:1704.06005 [hep-ph].
- [26] T. Abe, J. Kawamura, S. Okawa and Y. Omura, JHEP **1703**, 058 (2017) [arXiv:1612.01643 [hep-ph]].
- [27] B. Bhattacharya, D. London, J. M. Cline, A. Datta and G. Dupuis, Phys. Rev. D **92**, no. 11, 115012 (2015) [arXiv:1509.04271 [hep-ph]].
- [28] D. S. Akerib *et al.* [LUX Collaboration], Phys. Rev. Lett. **116**, no. 16, 161301 (2016) [arXiv:1512.03506 [astro-ph.CO]].

- [29] D. S. Akerib *et al.*, arXiv:1608.07648 [astro-ph.CO].
- [30] E. Aprile *et al.* [XENON Collaboration], arXiv:1705.06655 [astro-ph.CO].
- [31] ATLAS collaboration ,ATLAS-CONF-2016-096.
- [32] ATLAS collaboration ,ATLAS-CONF-2017-038.
- [33] ATLAS collaboration ,ATLAS-CONF-2017-022.
- [34] J. Alwall, R. Frederix, S. Frixione, V. Hirschi, F. Maltoni, O. Mattelaer, H.-S. Shao and T. Stelzer *et al.*, JHEP **1407**, 079 (2014) [arXiv:1405.0301 [hep-ph]].
- [35] C. Degrande, C. Duhr, B. Fuks, D. Grellscheid, O. Mattelaer and T. Reiter, Comput. Phys. Commun. **183**, 1201 (2012) [arXiv:1108.2040 [hep-ph]].
- [36] A. Alloul, N. D. Christensen, C. Degrande, C. Duhr and B. Fuks, Comput. Phys. Commun. **185**, 2250 (2014) [arXiv:1310.1921 [hep-ph]].
- [37] T. Sjostrand, S. Mrenna and P. Z. Skands, JHEP **0605**, 026 (2006) [hep-ph/0603175].
- [38] F. Caravaglios, M. L. Mangano, M. Moretti and R. Pittau, Nucl. Phys. B **539**, 215 (1999) [hep-ph/9807570].
- [39] J. de Favereau *et al.* [DELPHES 3 Collaboration], JHEP **1402**, 057 (2014) [arXiv:1307.6346 [hep-ex]].
- [40] M. Cacciari, G. P. Salam and G. Soyez, JHEP **0804**, 063 (2008) [arXiv:0802.1189 [hep-ph]].
- [41] ATLAS collaboration, ATL-PHYS-PUB-2015-037.
- [42] ATLAS collaboration, ATL-PHYS-PUB-2016-012.
- [43] S. Okawa and Y. Omura, arXiv:1703.08789 [hep-ph].
- [44] Y. Amhis *et al.* [Heavy Flavor Averaging Group (HFAG)], arXiv:1412.7515 [hep-ex].
- [45] S. Aoki *et al.*, Eur. Phys. J. C **77**, no. 2, 112 (2017) [arXiv:1607.00299 [hep-lat]].
- [46] A. J. Buras, M. Jamin and P. H. Weisz, Nucl. Phys. B **347**, 491 (1990).
- [47] C. Patrignani *et al.* [Particle Data Group], Chin. Phys. C **40**, no. 10, 100001 (2016).
- [48] CKMfitter global fit results as of Summer 2016 (ICHEP 2016 conference)
http://ckmfitter.in2p3.fr/www/html/ckm_main.html
- [49] A. Celis, J. Fuentes-Martin, A. Vicente and J. Virto, arXiv:1704.05672 [hep-ph].
- [50] D. Bardhan, P. Byakti and D. Ghosh, arXiv:1705.09305 [hep-ph].

- [51] E. Golowich, J. Hewett, S. Pakvasa and A. A. Petrov, Phys. Rev. D **76**, 095009 (2007) [arXiv:0705.3650 [hep-ph]].
- [52] A. A. Petrov, arXiv:1312.5304 [hep-ph].
- [53] Y. Amhis *et al.*, arXiv:1612.07233 [hep-ex].
- [54] N. Carrasco *et al.*, Phys. Rev. D **90**, no. 1, 014502 (2014) [arXiv:1403.7302 [hep-lat]].
- [55] G. Bélanger, F. Boudjema, A. Pukhov and A. Semenov, Comput. Phys. Commun. **192**, 322 (2015) [arXiv:1407.6129 [hep-ph]].
- [56] P. Agrawal, S. Blanchet, Z. Chacko and C. Kilic, Phys. Rev. D **86**, 055002 (2012) [arXiv:1109.3516 [hep-ph]].
- [57] M. Drees and M. Nojiri, Phys. Rev. D **48**, 3483 (1993) [hep-ph/9307208].
- [58] J. Hisano, K. Ishiwata and N. Nagata, Phys. Lett. B **706**, 208 (2011) [arXiv:1110.3719 [hep-ph]].
- [59] J. Hisano, R. Nagai and N. Nagata, JHEP **1505**, 037 (2015) [arXiv:1502.02244 [hep-ph]].